Ultrafast Hole Trapping and Relaxation Dynamics in p-Type CuS Nanodisks

ARTICLE *in* JOURNAL OF PHYSICAL CHEMISTRY LETTERS · JULY 2015

Impact Factor: 7.46 · DOI: 10.1021/acs.jpclett.5b01078 · Source: PubMed

THE JOURNAL OF PHYSICAL CHEMISTRY Letters

Letter

pubs.acs.org/JPCL

Ultrafast Hole Trapping and Relaxation Dynamics in p-Type CuS Nanodisks

John Ludwig,[†] Li An,[‡] Brian Pattengale,[†] Qingyu Kong,[§] Xiaoyi Zhang,*[,§] Pinxian Xi,*[,‡] and Jier Huang*[,†]

[†]Department of Chemistry, Marquette University, Milwaukee, Wisconsin 53201, United States

[‡]Key Laboratory of Nonferrous Metal Chemistry and Resources Utilization of Gansu Province, State Key Laboratory of Applied Organic Chemistry and The Research Center of Biomedical Nanotechnology, Lanzhou University, Lanzhou, Gansu 730000, People's Republic of China

[§]X-ray Science Division, Argonne National Laboratory, Argonne, Illinois 60349, United States

Supporting Information

ABSTRACT: CuS nanocrystals are potential materials for developing low-cost solar energy conversion devices. Understanding the underlying dynamics of photoinduced carriers in CuS nanocrystals is essential to improve their performance in these devices. In this work, we investigated the photoinduced hole dynamics in CuS nanodisks (NDs) using the combination of transient optical (OTA) and X-ray (XTA) absorption spectroscopy. OTA results show that the broad transient absorption in the visible region is attributed to the photoinduced hot and trapped holes. The hole trapping process occurs on a subpicosecond time scale, followed by carrier recombination (~100 ps). The nature of the hole trapping sites, revealed by XTA, is characteristic of S or organic ligands on the surface of CuS NDs. These results not only suggest the possibility to control the hole dynamics by tuning the surface chemistry of CuS but also represent the first time observation of hole dynamics in semiconductor nanocrystals using XTA.

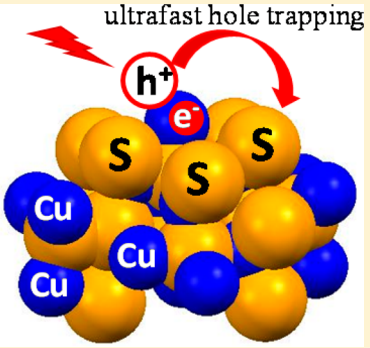

Copper sulfides ($Cu_{2-x}S$), well-known p-type semiconductors due to the stoichiometric deficiency of copper in the lattice, have attracted considerable attention because of their broad applications in diverse fields including photovoltaics, photocatalysis, batteries, chemical sensing, and electronics.[1−4] There are several stable $Cu_{2-x}S$ phases with the stoichiometric factor x ranging between 0 and 1, from the copper-rich chalcocite (Cu_2S) to the copper-deficient composition (CuS). Among them, the hexagonal covellite (CuS) is of particular interest due to its significant density of free carriers (holes) in the valence band accounting for its unique metallic conductivity and the strong localized surface plasmon resonance (LSPR) in NIR.[5−8] These characteristics, together with its suitable band gap (2.2 eV), make CuS potentially ideal as low-cost light-harvesting and charge-transport materials in photovoltaics and photocatalysis.[7,9−11]

The successful utilization of CuS nanocrystals in photocatalysis and photovoltaic devices largely depends on the trapping and relaxation dynamics of charge carriers in CuS nanocrystals. Due to the larger amount of surface states in nanocrystals compared to the bulk materials, the electrons and holes in nanocrystals can be readily trapped at those surface states after photoexcitation, which typically results into a decreased device performance. Therefore, a fundamental understanding of the charge carrier trapping and relaxation dynamics in CuS nanocrystals is essential to rationally design efficient CuS nanocrystals for CuS-based devices. Although the synthesis of size and shape-controllable CuS nanocrystals[5,10,12−14] and their LSPR properties have been extensively investigated in the past decade,[5,8,15] little is known about the spectral signatures and dynamics of photogenerated carriers in CuS nanocrystals.[16,17] In this work, we report the hole dynamics of CuS nanodisks (NDs) using the combination of optical (OTA) and X-ray (XTA) transient absorption spectroscopy. The ultrafast dynamics are explained in terms of hot hole relaxation and hole trapping into the localized states. The nature of the hole trapping state is elucidated by the XTA experiment, demonstrating that the holes are mainly trapped at S or surrounding ligands on the surface of NDs.

The monodisperse CuS NDs were synthesized using the solvothermal process, which involves the fast injection of sulfur/1-octadecene (ODE) solution into the CuCl/hexadecylamine (HDA) mixture.[18] Details of the synthesis are provided in the Supporting Information (SI). The morphology and structural features of CuS NDs are studied by transmission electron microscopy (TEM), and high-resolution TEM (HRTEM), and X-ray diffraction (XRD). Figure 1a displays the representative TEM images of as-prepared CuS NDs, from which the two-dimensional disk-like morphology can be immediately inferred. The CuS NDs lying flat on the supporting substrate of the TEM grid are hexagonal, while those standing on their lateral sidewalls on the substrate appeared to be rod-shaped (the inset of Figure 1a). The dimensions of CuS NDs are estimated to be 11.0 × 3.2 nm with

Received: May 25, 2015
Accepted: June 22, 2015

DOI: 10.1021/acs.jpclett.5b01078
J. Phys. Chem. Lett. 2015, 6, 2671−2675

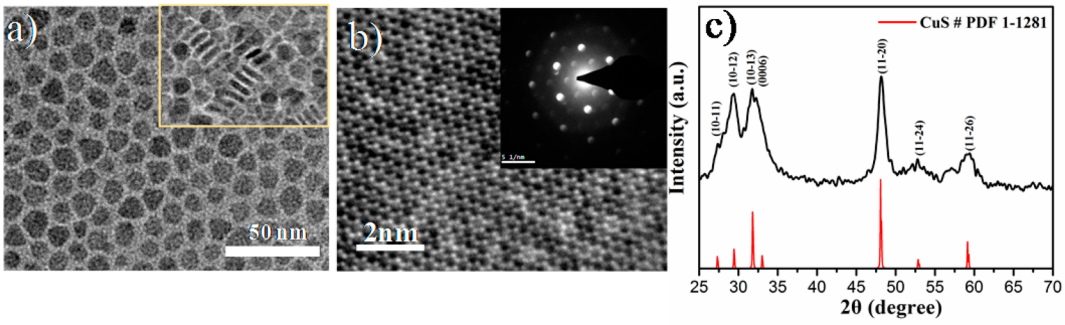

Figure 1. TEM image (a), HRTEM image (b), and XRD patterns (c) of CuS NDs. The inset of (b) shows the CBED pattern of CuS NDs. The red vertical lines in (c) show diffraction peaks reported for CuS bulk reference patterns.

an aspect ratio of 3.4. The HRTEM image (Figure 1b) taken from a single CuS ND together with its convergent beam electron diffraction (CBED) taken using a 10 nm beam spot size (inset of Figure 1b) indicates that the single CuS ND is single-crystalline. The XRD patterns acquired on dry powders of NDs (Figure 1c, black line) confirm the formation of hexagonal CuS with Cu/S = 1:1 stoichiometry (JCPDS-01-1281, *P*63/*mmc*).

The electronic state and chemical composition of the synthesized CuS NDs were analyzed by the combination of X-ray photoelectron spectroscopy (XPS) and X-ray absorption spectroscopy (XAS). The high-resolution XPS of Cu 2p of CuS NDs (Figure 2a) shows two strong peaks at 931.8 and 951.6

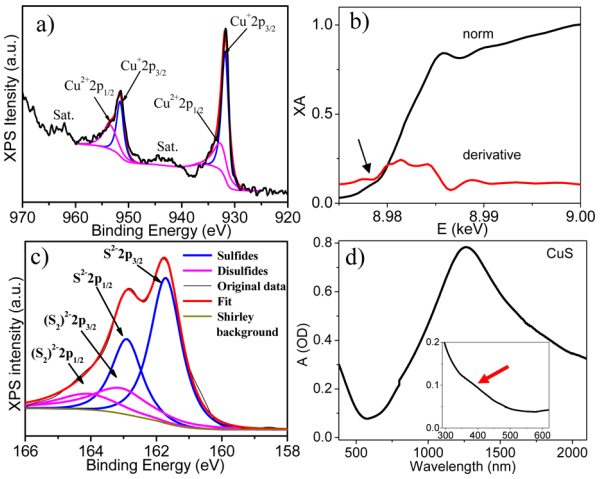

Figure 2. (a) High-resolution XP spectra of CuS NDs in the Cu 2p binding energy region. (b) The normalized (black) and derivative (red) Cu K-edge XAS spectra of CuS NDs. (c) High-resolution XP spectra of CuS NDs in the S 2p binding energy region. (d) Steady-state absorption spectrum of CuS NDs.

eV, which is consistent with the literature data of Cu^{+} $2p_{3/2}$ and $2p_{1/2}$[19] and can thus be attributed to Cu^{+} in CuS NDs. In addition, two low-intensity components on the high binding energy sides of Cu^{+} $2p_{3/2}$ and $2p_{1/2}$, that is, 932.7 and 953.5 eV, are consistent with the Cu^{2+} binding energy and thus can be assigned to the Cu^{2+} oxidation state.[21] The Cu^{2+} vacancy is further confirmed by the presence of the satellite peaks (marked as Sat. in Figure 2a), typical for the Cu +2 oxidation state.[20,21] These Cu 2p bands can be adequately fitted by four curve-fitting bands, representing Cu^{2+} and Cu^{+} $2p_{3/2}$ and $2p_{1/2}$, respectively, suggesting the presence of both Cu^{2+} and Cu^{+} vacancies. The presence of Cu^{2+} was further confirmed by XAS studies. As shown in Figure 2b, a pre-edge feature at ∼8979 eV, representative of the quadrupole 1s−3d transitions of the Cu center, was observed. Because the electronic configuration of Cu^{0} is $3d^{10}4s^{1}$, the quadrupole 1s−3d transition is only allowed if there is Cu^{2+} in NDs with a $3d^{9}$ configuration, consistent with XPS results. Figure 2c shows the high-resolution XP spectrum at the S 2p region. The deconvolution of the S 2p spectrum yields two main doublets at (161.7 eV, 162.9 eV) and (163.1 eV, 164.2 eV), which are typical values for metal sulfides and can be assigned to sulfide and disulfide, respectively.[9,22,23] All of the above results indicate that the ionic model of the CuS NDs is $(Cu_2)^{2+}(Cu)^{2+}(S_2)^{2-}(S)^{2-}$, consistent with the valence state of 4/3 for Cu in CuS nanocrystals reported previously.[24,25]

Figure 2d shows the UV−visible−NIR absorption spectrum of CuS NDs in toluene solution. The broad excitonic peak (Figure 2d inset) is observed in the UV−visible region with an absorption onset at ∼2.2 eV, which is strongly blue-shifted compared to the bulk reference, indicating a size quantization effect. In the NIR region, a well-defined absorption peak centered at 1261 nm is observed, which is characteristic of LSPR due to the presence of valence band free holes.

Figure 3a and b shows the OTA spectra of CuS NDs in toluene at early time (<2 ps) and later time (>2 ps), respectively, after 1000 nm excitation. The initial spectrum (t = 0.3 ps) is dominated by two absorption bands centered at 672 and 530 nm and a broad negative signal at >720 nm. These spectral features quickly (<2 ps) evolve to two broader absorption bands centered at 690 and 480 nm with the vanishing of the bleach signal. This evolution is accompanied by two isosbestic points located at ∼709 and 472 nm, suggesting that the spectral evolution within the 2 ps time window is due to the formation of new species. After 2 ps (Figure 3b), the spectrum decays with time and shows negligible spectral evolution. The early time spectral evolution can be further seen by comparing the kinetics traces at different probe wavelengths. As shown in Figure 3c (inset), the kinetic trace at long probe wavelength (650 nm) shows an instantaneous rise, that is, comparable to the pump pulse width, followed by a fast decay. In contrast, the kinetic traces at shorter wavelengths exhibit a rising component with its time constant increasing at shorter wavelength. These probe-wavelength-dependent features at early time (<2 ps) are followed by the identical decay at later time (Figure 3c), which is consistent with the spectral evolution observed earlier and suggests the conversion between two species at t < 2 ps and intrinsic decay afterward. The probe-wavelength-dependent decay kinetics has been observed in other semiconductors and is characteristic of a charge carrier

DOI: 10.1021/acs.jpclett.5b01078
J. Phys. Chem. Lett. 2015, 6, 2671−2675

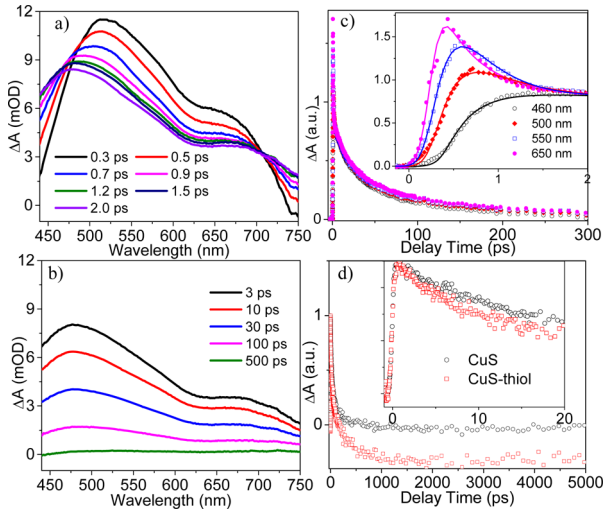

Figure 3. (a,b) OTA spectra of CuS NDs at early time (<2 ps) and later time (>2 ps), respectively, after 1000 nm excitation. (c) The comparison of OTA kinetic traces of CuS NDs at probe wavelengths of 460, 500, 550, and 650 nm after 1000 nm excitation. (d) The comparison of OTA kinetic traces at 460 nm for CuS NDs in the presence and absence of the hole scavenger (1-dodecanethiol).

trapping process.[26,27] Given that the excitation energy at 1000 nm (1.24 eV) is much lower than the band gap excitation energy (~2.2 eV) and can only excite the plasmonic mode (step 1 in Scheme 1), it is reasonable to assign the broad absorption in the whole visible window to the photoinduced hole signal in CuS NDs.

Scheme 1. Schematic Illustration of Carrier Dynamics in CuS NDs after 1000 (red arrows) and 400 nm (blue arrows, left) Excitation[a]

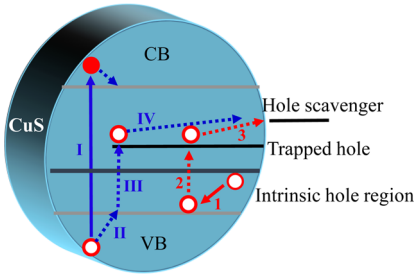

[a]After 1000 nm excitation (1), a hot hole is generated through exciting the plasmonic band, which is quickly followed by the hole trapping process (2). The 400 nm excitation generates a hot electron in the conduction band and a hot hole in the valence band (I). The hot hole in the valence bad quickly relaxes to the valence band edge (II) and is eventually trapped at the hole trapping site (III). In the presence of a hole scavenger, hole transfer occurs from the hole trapping site to the hole scavenger (3 and IV).

To further confirm that the broad absorption is due to the hole absorption, we measured the OTA spectra of CuS NDs in the presence of a hole scavenger, 1-dodecanethiol. As shown in Figure S1 (SI), at early time (<2 ps), the main spectral features and the kinetic trace of CuS NDs in the presence of 1-dodecanethiol appear to be identical to that of CuS NDs, suggesting that the hole trapping process is insensitive to the presence of a hole scavenger. At later time (>2 ps), however, the OTA spectra of CuS NDs in the presence of 1-dodecanethiol decay faster and eventually invert to a long-lived broad negative (bleach) signal at <700 nm (Figure S1 (SI) and Figure 3d). The accelerated decay of the broad absorption in CuS NDs due to the presence of a hole scavenger, which has been seen in other semiconductor nanocrystals,[28] unambiguously confirms the assignment of the broad absorption in the whole spectral window to hole absorption. The origin of the formation of the broad bleach signal in the presence of 1-dodecanethiol at later time (>100 ps) remains unclear to us. One possibility is that due to hole transfer from CuS NDs to 1-dodecanethiol (step 3, Scheme 1), the hole density in the valence band of CuS NDs is reduced. As a result, the transition probability for electrons from the deeper level of the valence band to the intrinsic hole region is reduced, giving rise to a broad bleach signal. This broad bleach signal is long-lived (≫5 ns, limited by our OTA setup window), indicating the slow charge recombination between CuS NDs and the hole scavenger.

These results all suggest that the initial broad absorption (centered at 672 and 530 nm) likely originated from the hot hole carriers after 1000 nm excitation, while the spectrum centered at 690 and 480 nm likely originated from the surface-trapped hole absorption. The kinetic traces in Figure 3c can all be fitted by a three-exponential function with the same time constants. Instead of three decay components of 0.44 (60%), 20.8 (24%), and 189 ps (16%) for the kinetic trace at 650 nm, the kinetic trace at 460 nm can be best represented by a rising component (0.44 ps) and two decay components, 20.8 (63%) and 189 ps (37%). The time constant of 0.44 ps can be attributed to the hole trapping process (step 2, Scheme 1), while the two decay components with 20.8 and 189 ps time constants can be assigned to the recombination of the charge carriers.

In addition to 1000 nm excitation, carrier dynamics after band gap excitation at 400 nm was also examined. As shown in Scheme 1, after band gap excitation, the electron in the valence band is promoted to the conduction band (step I), leaving a hole behind. In principle, we expect to see the signals resulting from the photoinduced electron in the conduction band in addition to the hole absorption. In contrast, the OTA spectra after band gap excitation (Figure S2, SI) resemble the spectra collected upon 1000 nm excitation, indicating that the OTA signals after band gap excitation are also dominated by the hole absorption with negligible contribution from photoinduced electrons in the conduction band. We believe that this is either due to significantly smaller extinction coefficient of photo-induced electrons than that of holes or the electron signal is outside of our probed spectral range. Analogous to 1000 nm excitation, the kinetic traces after band gap excitation are probe-wavelength-dependent (Figure S2, SI), suggesting that the hole trapping process occurs upon band gap excitation. However, the early time kinetic traces between two experiments are slightly different. Instead of instant rising at 650 nm after 1000 nm excitation, an ultrafast rising component was observed at 650 nm after 400 nm excitation. Because the energy of 400 nm is larger than the band gap (~525 nm), an extra relaxation process, that is, the electron/hole promoted to the higher levels of conduction/valence bands quickly relax to band gap edge (step II), was included. Therefore, the rising component observed at 650 nm after 400 nm excitation is likely due to the relaxation of hot carriers from a higher energy level to the band edge.

DOI: 10.1021/acs.jpclett.5b01078
J. Phys. Chem. Lett. 2015, 6, 2671−2675

The nature of the carrier trapping state was investigated by probing the Cu valence state using XTA. The XTA spectrum at the Cu K-edge was collected in fluorescence mode at the 11ID-D beamline of the Advanced Photon Source (APS). Figure 4a

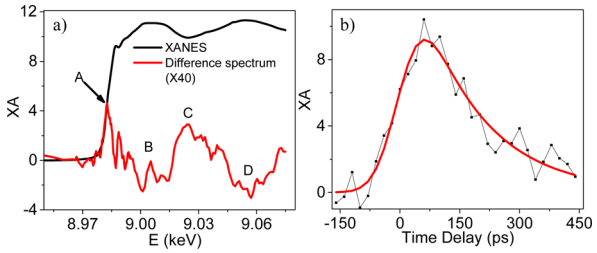

Figure 4. (a) XANES spectrum of CuS NDs at the Cu K-edge before laser excitation. The difference spectrum is obtained by subtracting the laser-off XANES spectrum from laser-on spectrum. Labels (A–D) indicate the main features observed in the difference spectrum. (b) The time dependence of the transient signal at 8.983 keV of CuS NDs.

shows the X-ray absorption near-edge structure (XANES) spectrum. The sharp peak at 8.986 keV corresponds to a 1s → $4p_z$ transition, while the broad transition between 8.99 and 9.01 keV results from the promotion of 1s to $4p_{x,y}$ unoccupied states. The peak at around 9.052 keV is mainly due to the scattering of the outgoing photoelectrons from the first coordination shell of S atoms. These features are consistent with Cu K-edge XAS of polycrystalline CuS powders reported by Kumar et al., which further confirms the CuS ionic model.[24] Also shown in Figure 4a is the transient X-ray absorption signal of CuS NDs (red plot), which is presented as the difference XANES spectrum obtained after subtracting the laser-off spectrum from the laser-on spectrum at 65 ps after 400 nm excitation. The positive feature (A) at 8.983 keV in the difference spectrum indicates that the Cu transition edge shifts to lower energy after laser excitation, suggesting photoinduced reduction at the Cu center. The full width at half-maximum (fwhm) of the X-ray probe is ~120 ps, and the hole trapping process occurs on the subpicosecond time scale, revealed by OTA. Therefore, the XTA spectrum collected at 65 ps after laser excitation measures the hole recombination dynamics after trapping is complete. Consequently, the observed Cu reduction indicates that the holes are removed from the Cu site and trapped at the surrounding S or ND ligands. Following the hole trapping process, the recombination of the trapped holes with electrons in the Cu site occurs, which was also captured by monitoring the intensity of the positive feature at 8.983 keV in the difference spectrum of CuS NDs (Figure 4b). The decay kinetics of the feature at 8.983 keV was fitted to a convolution of a Gaussian function, with the 120 ps fwhm representing the X-ray pulse and an exponential function representing the excited hole population. The lifetime of the excited hole was 154 ± 7 ps by fitting the XTA data, consistent with the above OTA results.

In addition to the positive feature A, a negative transient signal in the range of 8.99–9.01 keV (indicated as valley B in Figure 4a) implies the decreased 1s to $4p_{x,y}$ absorption intensity. The positive feature C and negative feature D in the difference spectrum are located around the valley and the peak of the oscillation of XANES spectrum, respectively. Because the oscillation at this region corresponds to the scattering from the first coordinate shell, the observed transient signals at C and D indicate the damping of the oscillation amplitude. The damping of the oscillation amplitude can be caused by elevated thermal or structure disorder. Because the X-ray pulse width is 120 ps and the thermal effect normally disappears after several picoseconds to 20 ps through vibrational cooling with the solvent, the damping of the oscillation amplitude is more likely due to the increased structure disorder after photon excitation.

In summary, we have examined the photoinduced carrier dynamics in monodispersed CuS NDs using the combination of OTA and XTA. OTA experiments unambiguously confirmed the photoinduced hole signal following the excitation of the plasmonic mode and band gap excitation. It was found that hole trapping occurs within subpicoseconds, which is followed by charge recombination with a ~100 ps time constant. XTA results revealed that the trap states are likely associated with S, which has a Cu deficiency, and/or the ligands on the surface of NDs, suggesting the possibility to control the hole dynamics by monitoring the surface structure or Cu stoichiometry. In addition, the ultrafast hole trapping process may compete with electron/hole recombination, the understanding of which will facilitate the study on the following charge transfer to electron/hole acceptors and thus provide guidance on their future application as light absorption and charge-transport materials for photovoltaics and photocatalysis.

■ ASSOCIATED CONTENT

Supporting Information

Material synthesis, sample preparation details, along with the experimental setup. The Supporting Information is available free of charge on the ACS Publications website at DOI: 10.1021/acs.jpclett.5b01078.

■ AUTHOR INFORMATION

Corresponding Authors

*E-mail: xyzhang@aps.anl.gov (X.Z.).
*E-mail: xipx@lzu.edu.cn (P.X.).
*E-mail: jier.huang@marquette.edu (J.H.).

Notes

The authors declare no competing financial interest.

■ ACKNOWLEDGMENTS

This work was supported by the Marquette University new faculty startup fund and China NSFC: 21201092 and Lzujbky-2014-m02. Use of the Advanced Photon Source and the Center for Nanoscale Materials at Argonne National Laboratory was supported by the U.S. Department of Energy, Office of Science, Office of Basic Energy Sciences, under Award No. DE-AC02-06CH11357. The femtosecond laser used in the XTA measurements was funded by a Midscale Instrumentation grant (DE-FG02-06ER06-13) from the Chemical, Biological and Geological Sciences Program, Basic Energy Science, Office of Science of the U.S. Department of Energy.

■ REFERENCES

(1) Wu, Y.; Wadia, C.; Ma, W. L.; Sadtler, B.; Alivisatos, A. P. Synthesis and Photovoltaic Application of Copper(I) Sulfide Nanocrystals. *Nano Lett.* **2008**, *8*, 2551–2555.

(2) Partain, L. D.; Mcleod, P. S.; Duisman, J. A.; Peterson, T. M.; Sawyer, D. E.; Dean, C. S. Degradation of a Cu_xS/CdS Solar-Cell in Hot, Moist Air and Recovery in Hydrogen and Air. *J. Appl. Phys.* **1983**, *54*, 6708–6720.

(3) Lou, Y. B.; Samia, A. C. S.; Cowen, J.; Banger, K.; Chen, X. B.; Lee, H.; Burda, C. Evaluation of the Photoinduced Electron Relaxation

DOI: 10.1021/acs.jpclett.5b01078
J. Phys. Chem. Lett. 2015, 6, 2671–2675

Dynamics of $Cu_{1.8}S$ Quantum Dots. *Phys. Chem. Chem. Phys.* **2003**, *5*, 1091−1095.
(4) Isac, L. A.; Duta, A.; Kriza, A.; Nanu, M.; Schoonman, J. Crystal Order in Cu_2S Thin Films Obtained by Spray Pyrolysis. *J. Optoelectron. Adv. Mater.* **2007**, *9*, 1265−1268.
(5) Xie, Y.; Carbone, L.; Nobile, C.; Grillo, V.; D'Agostino, S.; Della Sala, F.; Giannini, C.; Altamura, D.; Oelsner, C.; Kryschi, C.; Cozzoli, P. D. Metallic-Like Stoichiometric Copper Sulfide Nanocrystals: Phase- and Shape-Selective Synthesis, Near-Infrared Surface Plasmon Resonance Properties, and Their Modeling. *ACS Nano* **2013**, *7*, 7352−7369.
(6) Gainov, R. R.; Dooglav, A. V.; Pen'kov, I. N.; Mukhamedshin, I. R.; Mozgova, N. N.; Evlampiev, I. A.; Bryzgalov, I. A. Phase Transition and Anomalous Electronic Behavior in the Layered Superconductor CuS Probed by NQR. *Phys. Rev. B* **2009**, *79*, 075115.
(7) Yuan, K. D.; Wu, J. J.; Liu, M. L.; Zhang, L. L.; Xu, F. F.; Chen, L. D.; Huang, F. Q. Fabrication and Microstructure of p-Type Transparent Conducting CuS Thin Film and Its Application in Dye-Sensitized Solar Cell. *Appl. Phys. Lett.* **2008**, *93*, 132106.
(8) Luther, J. M.; Jain, P. K.; Ewers, T.; Alivisatos, A. P. Localized Surface Plasmon Resonances Arising from Free Carriers in Doped Quantum Dots. *Nat. Mater.* **2011**, *10*, 361−366.
(9) Zhang, Y. W.; Tian, J. Q.; Li, H. Y.; Wang, L.; Qin, X. Y.; Asiri, A. M.; Al-Youbi, A. O.; Sun, X. P. Biomolecule-Assisted, Environmentally Friendly, One-Pot Synthesis of CuS/Reduced Graphene Oxide Nanocomposites with Enhanced Photocatalytic Performance. *Langmuir* **2012**, *28*, 12893−12900.
(10) Basu, M.; Sinha, A. K.; Pradhan, M.; Sarkar, S.; Negishi, Y.; Govind; Pal, T. Evolution of Hierarchical Hexagonal Stacked Plates of CuS from Liquid−Liquid Interface and Its Photocatalytic Application for Oxidative Degradation of Different Dyes under Indoor Lighting. *Environ. Sci. Technol.* **2010**, *44*, 6313−6318.
(11) Ramasamy, K.; Malik, M. A.; Revaprasadu, N.; O'Brien, P. Routes to Nanostructured Inorganic Materials with Potential for Solar Energy Applications. *Chem. Mater.* **2013**, *25*, 3551−3569.
(12) Wu, C. Y.; Yu, S. H.; Chen, S. F.; Liu, G. N.; Liu, B. H. Large Scale Synthesis of Uniform CuS Nanotubes in Ethylene Glycol by a Sacrificial Templating Method under Mild Conditions. *J. Mater. Chem.* **2006**, *16*, 3326−3331.
(13) Zhu, H. T.; Wang, J. X.; Wu, D. X. Fast Synthesis, Formation Mechanism, and Control of Shell Thickness of CuS Hollow Spheres. *Inorg. Chem.* **2009**, *48*, 7099−7104.
(14) Yu, X. L.; Cao, C. B.; Zhu, H. S.; Li, Q. S.; Liu, C. L.; Gong, Q. H. Nanometer-Sized Copper Sulfide Hollow Spheres with Strong Optical-Limiting Properties. *Adv. Funct. Mater.* **2007**, *17*, 1397−1401.
(15) Zhao, Y. X.; Pan, H. C.; Lou, Y. B.; Qiu, X. F.; Zhu, J. J.; Burda, C. Plasmonic $Cu_{2-x}S$ Nanocrystals: Optical and Structural Properties of Copper-Deficient Copper(I) Sulfides. *J. Am. Chem. Soc.* **2009**, *131*, 4253−4261.
(16) Lou, Y. B.; Chen, X. B.; Samia, A. C.; Burda, C. Femtosecond Spectroscopic Investigation of the Carrier Lifetimes in Digenite Quantum Dots and Discrimination of the Electron and Hole Dynamics via Ultrafast Interfacial Electron Transfer. *J. Phys. Chem. B* **2003**, *107*, 12431−12437.
(17) Klimov, V. I.; Karavanskii, V. A. Mechanisms for Optical Nonlinearities and Ultrafast Carrier Dynamics in Cu_xS Nanocrystals. *Phys. Rev. B* **1996**, *54*, 8087−8094.
(18) Du, W. M.; Qian, X. F.; Ma, X. D.; Gong, Q.; Cao, H. L.; Yin, H. Shape-Controlled Synthesis and Self-Assembly of Hexagonal Covellite (CuS) Nanoplatelets. *Chem.—Eur. J.* **2007**, *13*, 3241−3247.
(19) Riha, S. C.; Johnson, D. C.; Prieto, A. L. Cu_2Se Nanoparticles with Tunable Electronic Properties Due to a Controlled Solid-State Phase Transition Driven by Copper Oxidation and Cationic Conduction. *J. Am. Chem. Soc.* **2011**, *133*, 1383−1390.
(20) Savariraj, A. D.; Viswanathan, K. K.; Prabakar, K. Influence of Cu Vacancy on Knit Coir Mat Structured CuS as Counter Electrode for Quantum Dot Sensitized Solar Cells. *ACS Appl. Mater. Interfaces* **2014**, *6*, 19702−19709.
(21) Zhang, J.; Yu, J. G.; Zhang, Y. M.; Li, Q.; Gong, J. R. Visible Light Photocatalytic H_2-Production Activity of CuS/ZnS Porous Nanosheets Based on Photoinduced Interfacial Charge Transfer. *Nano Lett.* **2011**, *11*, 4774−4779.
(22) Li, B. X.; Xie, Y.; Xue, Y. Controllable Synthesis of CuS Nanostructures from Self-Assembled Precursors with Biomolecule Assistance. *J. Phys. Chem. C* **2007**, *111*, 12181−12187.
(23) Kundu, M.; Hasegawa, T.; Terabe, K.; Aono, M. Effect of Sulfurization Conditions on Structural and Electrical Properties of Copper Sulfide Films. *J. Appl. Phys.* **2008**, *103*, 073523−073527.
(24) Kumar, P.; Nagarajan, R. Sarangi, R. Quantitative X-ray Absorption and Emission Spectroscopies: Electronic Structure Elucidation of Cu_2S and CuS. *J. Mater. Chem. C* **2013**, *1*, 2448−2454.
(25) Gu, J. B.; Wang, C. J.; Cheng, Y.; Zhang, L.; Yang, X. D. Probing the Structural and Electronic Properties of Boron Cluster Anions Doped with One or Two Aluminum Atoms. *Comput. Theor. Chem.* **2014**, *1049*, 67−74.
(26) Aiga, N.; Jia, Q. X.; Watanabe, K.; Kudo, A.; Sugimoto, T.; Matsumoto, Y. Electron−Phonon Coupling Dynamics at Oxygen Evolution Sites of Visible-Light-Driven Photocatalyst: Bismuth Vanadate. *J. Phys. Chem. C* **2013**, *117*, 9881−9886.
(27) Huang, Z. Q.; Lin, Y. J.; Xiang, X.; Rodriguez-Cordoba, W.; McDonald, K. J.; Hagen, K. S.; Choi, K. S.; Brunschwig, B. S.; Musaev, D. G.; Hill, C. L.; et al. In Situ Probe of Photocarrier Dynamics in Water-Splitting Hematite (α-Fe_2O_3) Electrodes. *Energy Environ. Sci.* **2012**, *5*, 8923−8926.
(28) Tang, J. W.; Durrant, J. R.; Klug, D. R. Mechanism of Photocatalytic Water Splitting in TiO_2. Reaction of Water with Photoholes, Importance of Charge Carrier Dynamics, and Evidence for Four-Hole Chemistry. *J. Am. Chem. Soc.* **2008**, *130*, 13885−13891.

DOI: 10.1021/acs.jpclett.5b01078
J. Phys. Chem. Lett. 2015, 6, 2671−2675